Pergamon

Bulletin of Mathematical Biology, Vol. 57, No. 5, pp. 651–677, 1995
Elsevier Science Ltd

0092-8240/95 $9.50 + 0.00

0092-8240(95)00023-2

DENSITY AND DIFFUSION LIMITED AGGREGATION IN MEMBRANES

■ JES STOLLBERG
Békésy Laboratory of Neurobiology,
University of Hawaii at Manoa,
Honolulu, HI 96822-2359, U.S.A.

(*E.mail: jesse@wana.pbrc.hawaii.edu*)

Aggregation of membrane molecules is a crucial phenomenon in developing organisms, a classic example being the aggregation of post-synaptic receptors during synaptogenesis. Our understanding of the molecular events involved is improving, but most models of the aggregation or concentration process do not address binding events on the molecular level. An exception is the study of diffusion limited aggregation, in which the aggregation process is simulated on a molecular level. In this analysis, however, important physical parameters such as molecular size, diffusion constant and initial density are not addressed. Thus no predictions about the rate at which such aggregates will form is possible. In the present work the model of diffusion limited aggregation is extended to incorporate these parameters and make the corresponding predictions.

1. Introduction. Many important cellular processes involve the aggregation of molecules diffusing in the plane of the membrane. The localization of acetylcholine receptors and other components at the developing neuromuscular junction is a well studied example in which aggregation is thought to proceed via a diffusion trap mechanism (Axelrod *et al.*, 1976; Edwards and Frisch, 1976; Anderson and Cohen, 1977; Chao *et al.*, 1981; Stollberg and Fraser, 1988). Considerable attention has been given to understanding the behavior diffusion trap models. Typically the analyses involve calculations of the flux of molecules due to density gradients over succeeding time increments, and are based on arbitrarily defined trapping regions with stipulated diffusion rates and trapping probabilities (Edwards and Frisch, 1976; Gershon, 1978; Chao *et al.*, 1981; Weaver, 1983; Stollberg and Gordon, 1992). Although useful in many ways these models do not address and therefore cannot test questions concerning molecular mechanism. Thus questions such as the number of molecular species involved, the stoichiometry of binding events, or the ultrastructure of the aggregated molecules lie outside the realm of this approach.

A quite different model of aggregation has been extensively studied within the physics and mathematics communities. This model has been termed

diffusion limited aggregation (DLA: Witten and Sander, 1981). In this family of models the behavior of individual particles are simulated (rather than their densities), and properties such as binding stoichiometry and aggregate structure are addressed. However there is no formulation for the initial density of particles or the rates of aggregation or diffusion, so that questions concerning the rate of growth of aggregates cannot be posed. The subject of this paper is an extension of the classic DLA model which will be termed density and diffusion limited aggregation (DDLA). This extension incorporates spatial and temporal considerations on the classic DLA model, thus permitting a study of the biologically interesting interactions between density, diffusion constant, and rate of aggregate growth.

2. Model Description—Classical DLA. Since the first report on diffusion limited aggregation (Witten and Sander, 1981) the simplicity of the assumptions involved have triggered a substantial literature on the subject (Witten and Sander, 1981; Muthukumar, 1983; Tokuyama and Kawasaki, 1984; Meakin, 1987; Mandelbrot and Evertsz, 1990; Ossadnik, 1991; Stenberg and Bygren, 1991; see also Kolb *et al.*, 1983; Meakin, 1983; Witten and Meakin, 1983; Saxton, 1992, 1993 for related studies of DLA at multiple sites and cluster–cluster aggregation). The essential elements of classical DLA are as follows (for a non-specialist introduction see Sander, 1986). Consider a grid (Fig. 1A) on which particles are free to diffuse. For our purposes the grid represents a cell membrane and the particles are membrane bound molecules. To initiate the aggregation, one particle is fixed to the grid by unspecified mechanism and "activated", so that it will bind other particles that happen to diffuse into apposition. For the present we assume that each particle can bind four other particles (valence = 4). Now a new particle is placed at random on the periphery of the grid, and is allowed to "diffuse" at random. Typically diffusion is modeled by use of a pseudo-random number generator to determine whether the particle moves 1 diameter up, down, left, or right, although other "step geometries" are also possible (see below). The grid is assumed to be large, and it is also common to impose periodic boundary conditions ("wrap-around"), so that a particle diffusing off the grid reappears on the opposite edge. Eventually the diffusing particle will move into one of the four locations from which it can bind the central particle irreversibly; it then becomes bound and can itself bind additional particles. At this point in the simulation a new particle is placed at random on the periphery of the grid, and the procedure is repeated (Fig. 1A).

Simulation of this aggregation process (and corresponding physics experiments) have been extensively studied (Meakin, 1987; Dewey and Datta, 1989; Moireira *et al.*, 1989; Mandelbrot and Evertsz, 1990; Ossadnik, 1991). Experimental clusters differ from each other because the initial conditions are

not exactly reproducible, and corresponding variation in simulations is observed when the random number generator (which controls the placement of new particles, as well as their diffusion) is initialized differently. There are however properties which are preserved (on average) from simulation to simulation and experiment to experiment. The best studied of these preserved properties is the fractal dimension, defined in terms of the relationship between the density of bound particles and the distance from the origin. It is a feature of these aggregates (when produced on a large scale) that the average number of particles within a circle of radius R is proportional to $R^{\sim 5/3}$; hence these structures are said to have a fractal dimension of 5/3 (Witten and Sander, 1981; Muthukumar, 1983; Tokuyama and Kawasaki, 1984).

From a biological perspective, DLA is an interesting but incomplete model for aggregation in a membrane. The interest is due to the fact that biologically relevant binding is often diffusion limited, and the molecular level of the analysis permits testable predictions about structure. However there is no information in such a model regarding the rate at which a diffusion limited aggregate will grow. This is a matter of some concern to biologists confronted with supra-molecular aggregates, as detected for example with fluorescence microscopy. In this situation it is often possible to estimate the rate of growth of the aggregate although information about the underlying structure is unavailable. If it could be determined that the observed growth rate was significantly different from that predicted, one could conclude that a DLA-like process does not account for the aggregation. However as there is no formulation for the diffusion constant and initial site density in classical DLA it cannot be used to predict rates of growth. It is with these questions in mind that the classic model of diffusion limited aggregation has been extended to density and diffusion limited aggregation (DDLA).

3. Model Description—DDLA. As we have seen, classical DLA requires the specification of 1 physical parameter (particle valence) and one simulation parameter (step geometry). For diffusion and density limited aggregation three additional physical parameters must be specified: the particle diameter, the particle diffusion constant, and the particle density. For example consider a membrane molecule with a diameter of 0.008 μm and a diffusion constant of 0.12 $\mu m^2\ sec^{-1}$, at a density of 100 μm^{-2} in a region of membrane. The initial strategy is to impose a grid of spacing 1 diameter ($g = 0.008\ \mu$m), so that for a given grid width the number of particles present can be calculated from the density. Thus a 1024×1024 grid will contain $100\ \mu m^{-2} \cdot (1024\ g)^2 \cdot (0.008\ \mu m\ g^{-2})^2 \approx 6711$ particles; these are randomly placed on the grid at the beginning of the simulation process. Each particle is taken through a single diffusion step, checked for binding, then each takes another diffusion step, and so on. The introduction of the diffusion constant can be accomplished by calculating the

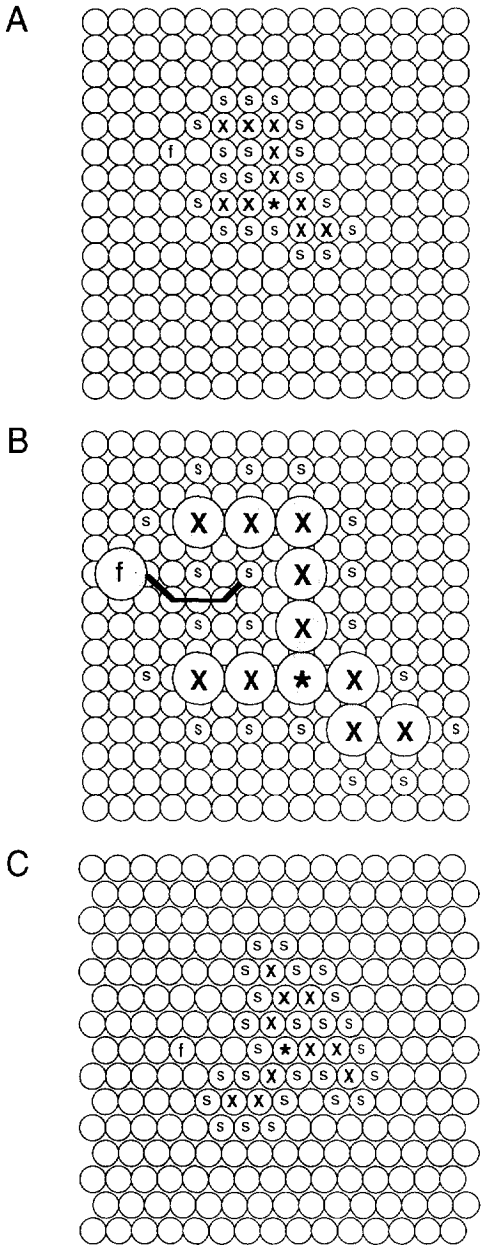

Figure 1.

mean square displacement of a single step. Consider the case where diffusion is modeled as a step of distance g (the grid spacing) up, down, left, or right (step geometry = 4; see Fig. 1A). The mean-square displacement for one step in this case is

$$\bar{X}^2 = \frac{4(1)^2}{4} g^2 = g^2.$$

Another simple scheme is to model diffusion as a particle moving to any of eight neighboring squares (adding diagonal steps to the above; step geometry = 8). In this case the mean-square displacement is

$$\bar{X}^2 = \frac{4(1)^2 + 4(\sqrt{2})^2}{8} g^2 = 1.5 \cdot g^2.$$

On a two-dimensional surface the mean-square displacement is related to the diffusion constant by

$$\bar{X}^2 = 4 \cdot D \cdot t,$$

which gives

$$t = \frac{g^2}{4 \cdot D} \text{ for step geometry} = 4,$$

or

$$t = \frac{1.5 \cdot g^2}{4 \cdot D} \text{ for step geometry} = 8.$$

In the above equations t gives the amount of time that corresponds to one elementary diffusion step; $t \approx 1.33 \times 10^{-4}$ sec in the above example for step geometry = 4. The number of elementary steps required to simulate 1 sec is thus $1/t = 7500$ steps.

Figure 1. Representation of the schemes by which density and diffusion limited aggregates are modeled. The diffusion grid is represented by the arrays of small circles; it is assumed that the particles diffuse by randomly stepping to adjacent circles. The origin in each figure is marked by "*", particles which have become trapped by "X", locations at which a particle could become stuck by "s", and freely diffusing particles by "f". A, One possible aggregate of 11 particles formed with the simplest simulation scheme. Particles are assumed to have a valence of 4, and the particle diameter is the size of the minimum diffusion step (scale 1 simulation). B, representation of the same structure at scale 2. In this case the particle diameter is twice the size of the minimal diffusion step. The aggregate structure shown is identical to that shown in A. Notice that a freely diffusing particle may bind to an inner sticky site in Fig. 1B, while the same site is protected in a scale 1 simulation (Fig. 1A). This may explain the tendency of higher scale simulations to be more dense than scale 1 simulations (see Discussion). C, representation of a hexagonal simulation (valence 6: step geometry 6) at scale 1. The array is represented in computer memory just as in A, but diffusion and binding rules are modified such that each row is interpreted to be offset from the row above by 1/2 of the grid spacing.

It is not immediately apparent whether a step geometry of four or eight is a better model for diffusion. A step geometry of four has the advantage that all the steps are of equal length, while adding the diagonal steps (step geometry = 8) confers more radial uniformity on the process. Of course other possibilities could be considered, e.g. imposing a finite probability that a particle would not move at all in a given diffusion step.

The best solution to this problem is to scale the diffusion step size so that with each elementary diffusion step the particles move a fraction of their diameter (Fig. 1B). This will be referred to as "scaled diffusion"—the scheme outlined above will be termed "scale 1" (step size = 1 diameter) and is compared with results from scale 2 and scale 4 simulations (step size = 1/2 or 1/4 diameter). These scaled diffusion models take more time and memory to run, but have the intuitive advantage that the spatially continuous process of diffusion can be more accurately approximated. As will be seen this is true regardless of the particular step geometry employed.

At issue then is how the typical aggregate structure and the average rate of growth depend on diffusion geometry and scale (simulation parameters), and binding valence and initial density (physical parameters). For completeness the diffusion constant should be added to the list of physical parameters, but from the model description it is clear that it enters into the simulations only as a coefficient relating diffusion steps to time. Thus a doubling of the diffusion constant causes a simulation to go through the same events in the first 30 sec that would have taken 60 sec previously.

All simulations reported here were performed on a grid of 1024×1024 particle diameters with periodic boundary conditions. This grid was found to be large enough to approximate the results on an infinite sheet under the given conditions, and should also be a good approximation to a small (near planar) region of a cell surface. Two modifications to the scheme outlined above were employed for simplicity and speed of simulation. First, only those particles close to the growing aggregate were subjected to single step diffusion. More remote particles were tagged for periodic updating, at which time the direction was selected by uniform random deviates, and the distance by a Gaussian random deviate scaled in accordance with the equation cited above and the elapsed time. Several simulations were run with and without this macro-diffusion feature and no significant differences were found. Second, freely diffusing particles were allowed to "diffuse through" each other (this happens implicitly in the macro-diffusion treatment, and was also allowed in single step diffusion). Even at the highest densities studied there should be little hindered diffusion (0.0256 is the largest "area fraction of obstacles", for comparison with Saxton, 1993), and there should be no net effect on the radial diffusion towards the growing aggregate.

The simulations are based on a standard molecule of diameter = 0.008 μm,

diffusion constant $= 0.12\ \mu m^2\ sec^{-1}$, and initial density 100 particles μm^{-2}. These values are taken as representative of some membrane molecules (e.g. the acetylcholine receptor: Poo, 1982; Stollberg and Fraser, 1990), and interpreting the results using these conventional units for distance will make the presentation more concrete. However the literature suggests a rather wide variation in measured diffusion rates, depending of course on the preparation but also on technique (Angelides *et al.*, 1988; Dubinsky *et al.*, 1989; Joe and Angelides, 1993; Kusumi *et al.*, 1993). Accordingly the reader may find use for data presented in terms of particle diameter (p) as the fundamental unit of distance. Thus the standard molecules considered in this work can be thought of as having a diameter of p, a diffusion constant of $1875\ p^2\ sec^{-1}$, at a density of $0.0064\ p^{-2}$. The advantage of these units is that results are more easily translated for molecules with different size and diffusion constant. For example a molecule of $0.004\ \mu m$ diameter with $D = 0.01\ \mu m^2\ sec^{-1}$ at a density of $200\ \mu m^{-2}$ corresponds to: diameter $= p$, $D = 625\ p^2\ sec^{-1}$ at a density of $0.0032\ p^{-2}$. This is identical to the standard molecule except that the density has been halved, and the diffusion constant altered. Simulations for the standard molecule at half the standard density are presented (Fig. 6; hollow circles), and the reader may take it that the new molecule will aggregate as depicted there except for the change in diffusion constant. As discussed above, the diffusion constant simply determines the proportionality constant relating diffusion steps and time, so the answer is that the new molecule will aggregate as that of Fig. 6 but at 625/1875 times the rate.

4. Results. The first question to be addressed concerns the method by which diffusion is modeled—whether one of the step geometries is to be preferred over the other. The mass growth rate of aggregates is shown in Fig. 2. Several important points are illustrated by Fig. 2A and B. First, the (scale 1) step geometry 4 simulations grow slightly faster than those of step geometry 8. Second, increasing the scale of the simulations introduces some change, but the result appears asymptotic as scale increases, so that scale 4 simulations are quite similar to scale 2 simulations. Third, the apparent asymptotic (scale 4) values for step geometry 4 simulations are nearly the same as for step geometry 8 (scale 4) simulations (Fig. 2A vs B). The valence 6 simulations show the first two trends clearly (slower growth as scale increases, and asymptotic scaling effect; Fig. 2C). It is interesting to note for comparison below that the rate at which mass increases with time is nearly the same for valence 4 and valence 6 simulations (at scale 4).

The average radial growth of aggregates is shown in Fig. 3 in terms of maximum radius and mean accretion radius as a function of time (Fig. 3, legend). Here the trends with increasing scale are the same as for mass growth: rate decreases with increasing scale, and the effects of scale are asymptotic. As

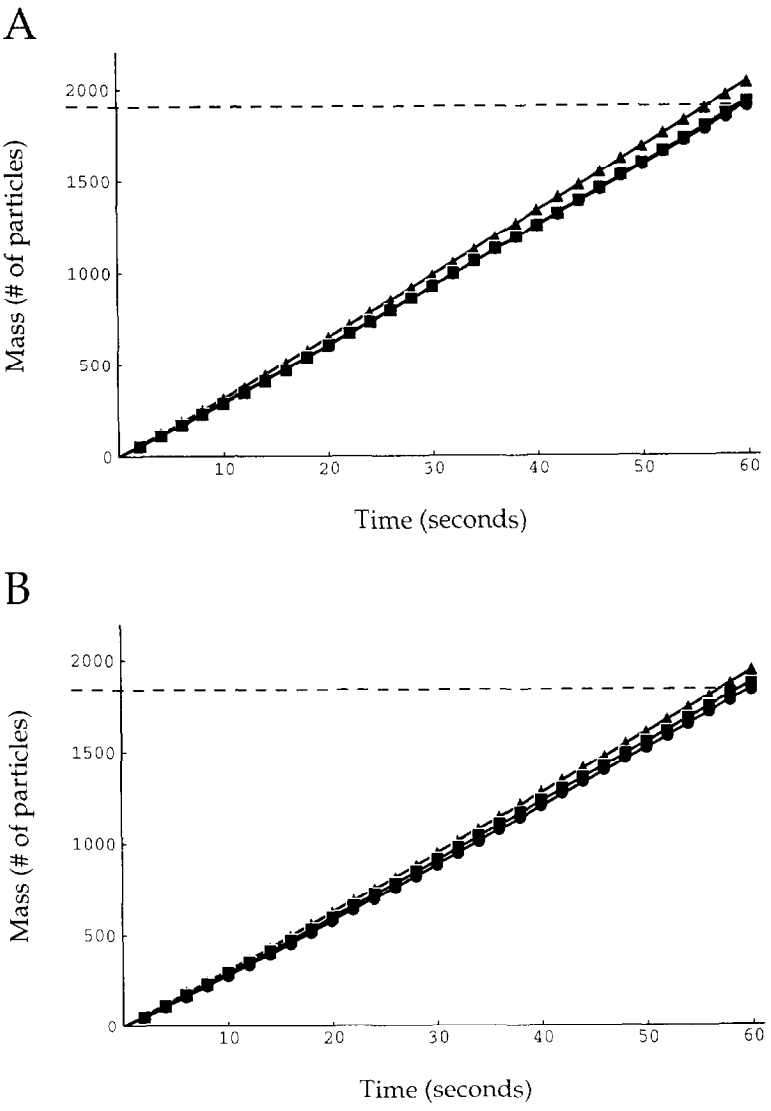

Figure 2. (A) and (B).

was seen with mass growth, it appears that scale 4 simulations are sufficiently high in scale to yield similar results regardless of step geometry (Fig. 3A vs B). There is a clear distinction between the two kinds of growth where valence is concerned, however. In terms of mass, valence 6 simulations increase at roughly the same rate as valence 4 (Fig. 2A,B vs C), but valence 6 aggregates grow significantly faster in terms of radius (Fig. 3A,B vs C).

A third way to characterize the different models under study is by the structure which results, in particular by the radial density of trapped particles.

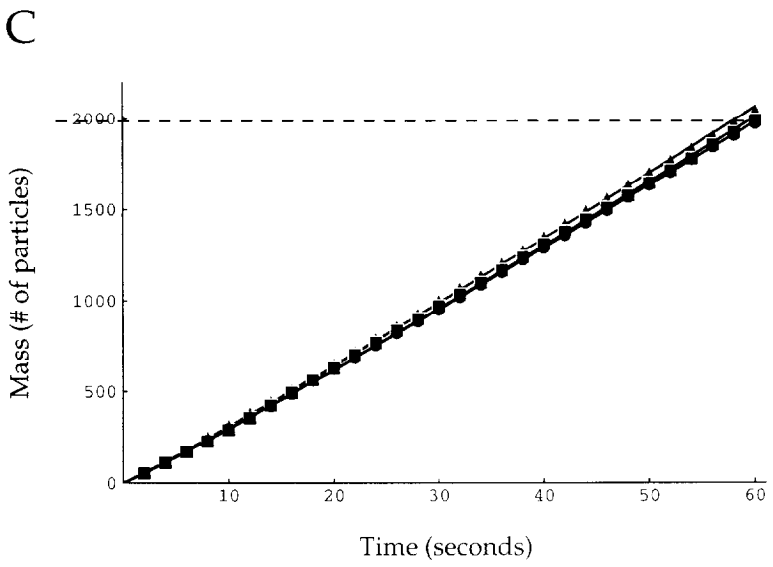

Figure 2. (C).

Figure 2. Comparison of the mass growth rates of density and diffusion limited aggregates using different models of step geometry and valence. Mass (the number of particles in the aggregate) is plotted vs time (seconds of physiological time) for aggregates formed under different conditions. The different scales of diffusion are indicated by triangles (scale 1), squares (scale 2), and circles (scale 4). Each point represents the mean and standard error of eight simulations. A, valence 4: step geometry 4. B, valence 4: step geometry 8. C, valence 6: step geometry 6. The mass growth rate decreases with increasing scale and/or step geometry, but all such differences are diminished as the scale increases. The curves represent Levenberg–Marquardt fits to mass$(t) = a \cdot t^b$; this form was chosen simply because it fit the data quite well. In this and subsequent figures the curves fitted are coded in terms of v_g_s_ where v is for valence, g for step geometry, and s for scale. Dashed lines, asymptotic (scale 4) values. A, v4g4s1: $5.19 \cdot t^{0.60}$, reduced $\chi^2 = 0.46$; v4g4s2: $4.35 \cdot t^{0.62}$, reduced $\chi^2 = 0.21$; v4g4s4: $4.31 \cdot t^{0.61}$, reduced $\chi^2 = 0.41$. B, v4g8s1: $4.63 \cdot t^{0.61}$, reduced $\chi^2 = 0.57$; v4g8s2: $4.34 \cdot t^{0.61}$; reduced $\chi^2 = 0.31$, v4g8s4: $4.01 \cdot t^{0.62}$, reduced $\chi^2 = 0.58$. C, v6s1: $5.81 \cdot t^{0.60}$, reduced $\chi^2 = 0.57$; v6s2: $4.94 \cdot t^{0.63}$, reduced $\chi^2 = 0.82$; v6s4: $4.77 \cdot t^{0.63}$, reduced $\chi^2 = 0.50$.

A useful way to measure this is to plot the included mass vs radius, i.e. the number of particles within a circle centered on the origin vs the radius of the circle. These plots are shown in Fig. 4. Once again the trend is toward asymptotic values as scale is increased. Again the asymptotic (scale 4) values are nearly the same for step geometry 4 vs step geometry 8 (Fig. 4A vs B). Finally, the radial density is significantly lower for valence 6 simulations than for those of valence 4 (Fig. 4A,B vs C). This is an expected finding; given that the mass growth rate is about the same (Fig. 2A,B vs C) while the radial growth is larger for valence 6 (Fig. 3A,B vs C), the valence 6 simulations would have to be less dense (see Discussion).

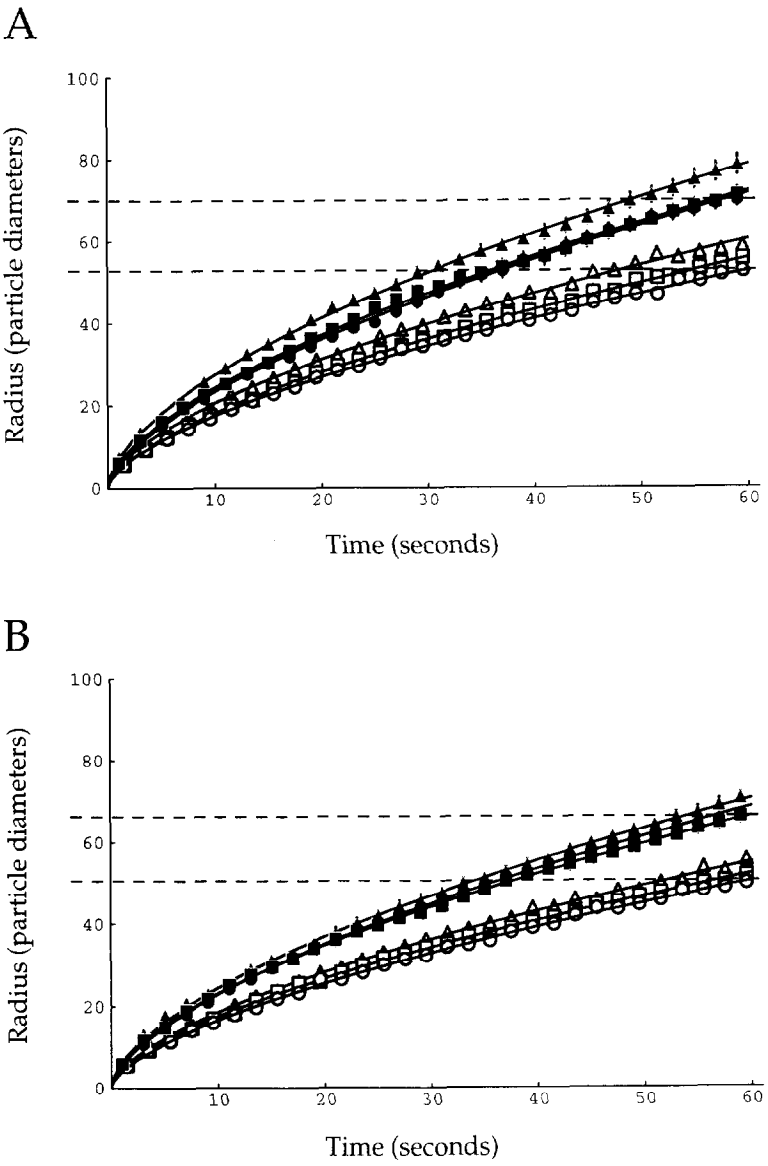

Figure 3. (A) and (B).

In order to make these observations more concrete the results of several simulation sets are shown in Fig. 5. In each part of the figure a typical aggregate grown for 60 sec of physiological time is shown along with two circles representing the mean accretion radius and the mean maximal radius for eight simulations after 60 sec. Figures 5A and B show the small but significant difference between step geometry 4 simulations of scale 1 (A, less compact) and

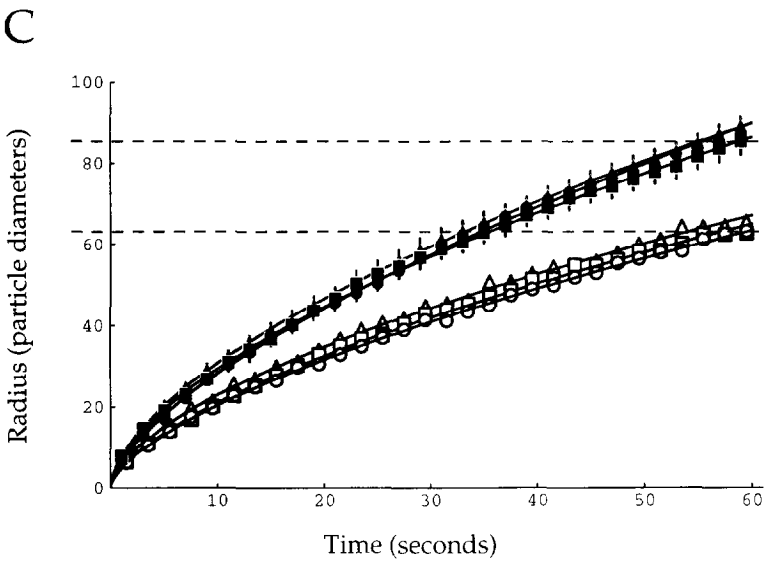

Figure 3. (C).

Figure 3. Comparison of the radial growth rates of density and diffusion limited aggregates using different models of step geometry and valence. Radius (in particle diameters) is plotted vs time (seconds of physiological time) for aggregates formed under different conditions. Two measures of radius are given; the maximal radius (solid symbols) and the mean radius of accretion over the previous second (hollow symbols). Each point represents the mean and standard error of eight simulations. The different scales of diffusion are indicated by triangles (scale 1), squares (scale 2), and circles (scale 4). A, valence 4: step geometry 4. B, valence 4: step geometry 8. C, valence 6: step geometry 6. Within each figure the radial growth rate is consistently lower as the diffusion scale increases (A, B, C). Comparison of step-geometries for valence 4 shows that step geometry 8 (B) produces a lower radial growth rate than step geometry 4 (A). This difference is most pronounced at scale 1, intermediate at scale 2, and very small at scale 4. Even at scale 4 there is a large difference between the radial growth of valence 4 and valence 6 simulations (A, B vs C). Because the step geometry has little effect at scale 4, this difference is attributed to the different valences. The curves represent Levenberg–Marquardt fits to radius $(t) = a \cdot t^b$; this form was chosen simply because it fit the data quite well. Dashed lines, asymptotic (scale 4) values. A, v4g4s1: $7.12 \cdot t^{0.59}$, reduced $\chi^2 = 0.37$; v4g4s2: $6.03 \cdot t^{0.61}$, reduced $\chi^2 = 0.22$; v4g4s4: $5.59 \cdot t^{0.62}$, reduced $\chi^2 = 0.24$. B, v4g8s1: $6.30 \cdot t^{0.59}$, reduced $\chi^2 = 0.31$; v4g8s2: $6.00 \cdot t^{0.59}$, reduced $\chi^2 = 0.09$; v4g8s4: $5.65 \cdot t^{0.61}$, reduced $\chi^2 = 0.22$. C, v6s1: $7.84 \cdot t^{0.60}$, reduced $\chi^2 = 0.03$; v6s2: $7.39 \cdot t^{0.60}$, reduced $\chi^2 = 0.19$; v6s1: $6.42 \cdot t^{0.64}$, reduced $\chi^2 = 0.59$.

scale 4 (B, more compact). In Fig. 5C and D the two scales of step geometry 8 simulations are shown, and although the trend is the same as for step geometry 4, the difference between scale 1 and scale 4 is smaller. Figure 5E and F makes the same comparison of scale for valence 6 simulations. Again the trend is the same, but the difference is smaller than for step geometry 4 simulations. A comparison of step geometries for valence 4 particles shows

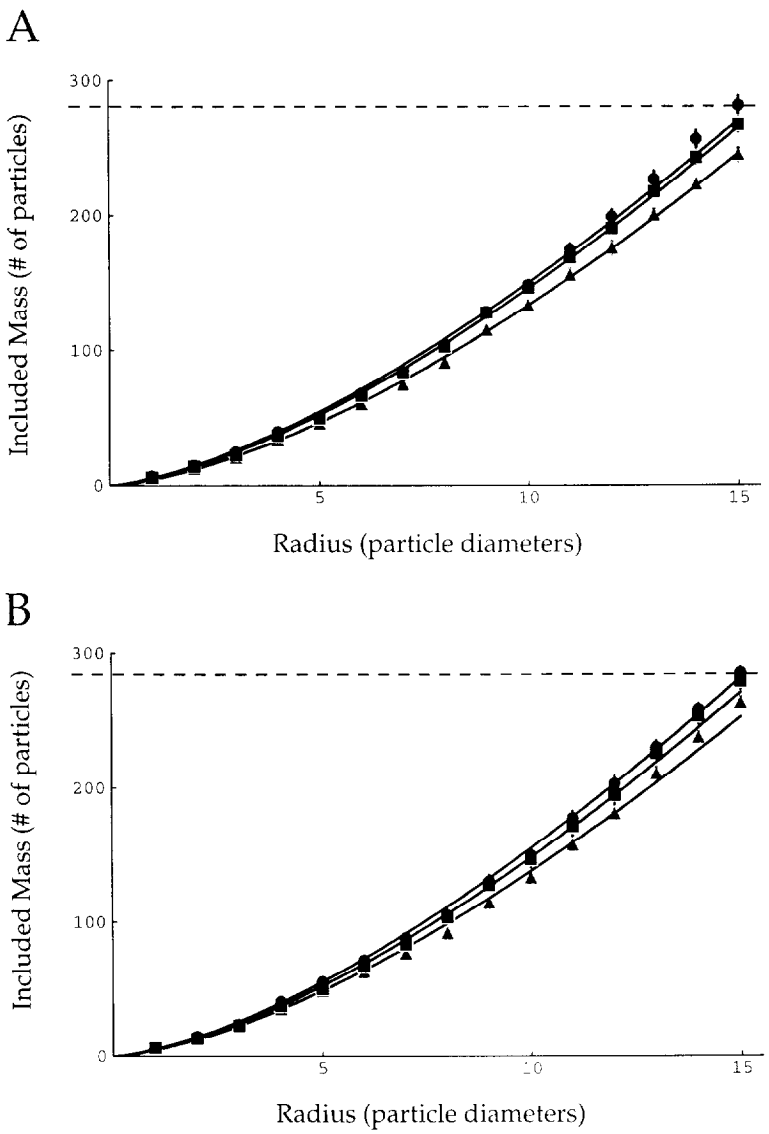

Figure 4. (A) and (B).

quite similar structures (Fig. 5B vs D), both of which are much more compact than the scale 4 valence 6 aggregates (Fig. 5F).

The final issue for consideration is that of initial particle density. Recall that one of the features of density and diffusion limited aggregation is that this initial density is a parameter of the simulation. Thus far we have considered only a fixed initial density (100 μm^{-2} or 0.0064 p^{-2}). It seems plain that an aggregate should grow more quickly as the initial density increases, but it is by no means

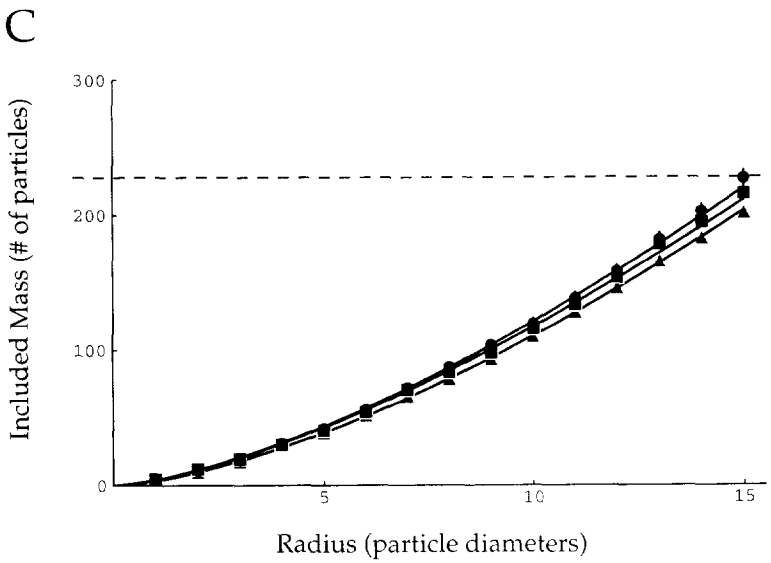

Figure 4. (C).

Figure 4. Comparison of the radial density of density and diffusion limited aggregates using different models of step geometry and valence. Included mass (number of particles within a circle of radius r, centered about the origin) is plotted vs r (radius in particle diameters) for aggregates formed under different conditions. The analysis was confined to the central region of the aggregates to ensure that the results were not contaminated by regions which were still being filled in when the simulations were terminated. Each point represents the mean and standard error of eight simulations. The different scales of diffusion are indicated by triangles (scale 1), squares (scale 2), and circles (scale 4). A, valence 4: step geometry 4. B, valence 4: step geometry 8. C, valence 6: step geometry 6. Within each figure the radial density is consistently higher as the diffusion scale increases (A, B, C). Comparison of step-geometries for valence 4 shows that step geometry 8 (B) produces a higher radial density than 4 (A). This difference is most pronounced at scale 1, intermediate at scale 2, and small at scale 4. Even at scale 4 there is a large difference between the radial density of valence 4 and valence 6 simulations (A, B vs C). Because the step geometry has little effect at scale 4, this difference is attributed to the different valences. The curves represent Levenberg–Marquardt fits to included mass$(r) = a \cdot r^b$; this form was chosen because it has been used in analysis of diffusion limited aggregation, and because it fits the data reasonably well. Dashed lines, asymptotic (scale 4) values. A, v4g4s1: $4.10 \cdot r^{1.51}$, reduced $\chi^2 = 1.19$; v4g4s2: $4.87 \cdot r^{1.48}$, reduced $\chi^2 = 2.00$; v4g4s4: $5.28 \cdot r^{1.45}$, reduced $\chi^2 = 3.64$. B, v4g8s1: $4.49 \cdot r^{1.49}$, reduced $\chi^2 = 5.15$; v4g8s2: $4.81 \cdot r^{1.49}$, reduced $\chi^2 = 4.03$; v4g8s4: $5.22 \cdot r^{1.47}$, reduced $\chi^2 = 2.29$. C, v6s1: $3.49 \cdot r^{1.50}$, reduced $\chi^2 = 0.33$; v6s2: $4.18 \cdot r^{1.45}$, reduced $\chi^2 = 1.93$; v6s1: $4.12 \cdot r^{1.47}$, reduced $\chi^2 = 1.23$.

clear how much faster, or what the consequences on aggregate structure might be. To investigate these matters simulations (valence 4, step geometry 8, scale 4) were performed at a range of initial densities; the mass as a function of time for the different initial densities is shown in Fig. 6. Figure 6A and B

A

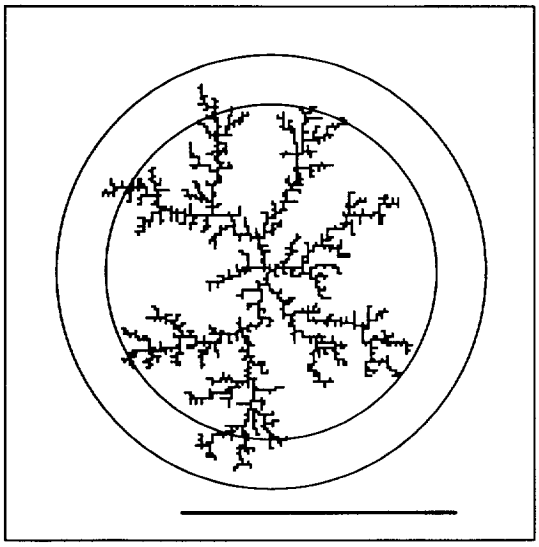

B

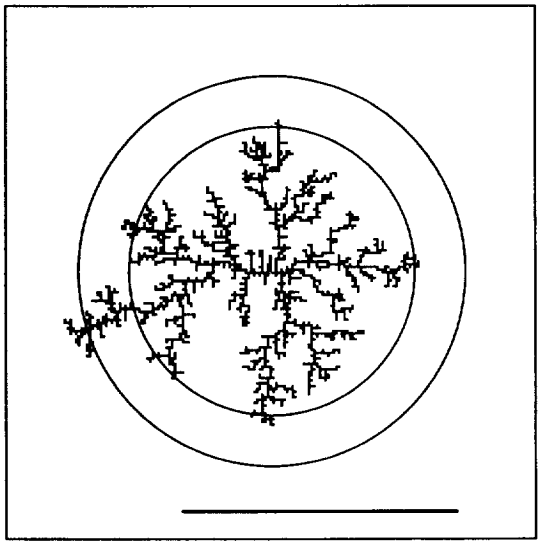

Figure 5. (A) and (B).

represent the same data set at different ordinate scales to give perspective on the data. It is clear that large initial densities lead to much faster growth than smaller ones, although the exact relationship between density and rate of growth is unclear. Figure 6C shows the same data with a logarithmic ordinate. It appears that each doubling of the density increases the log of the mass by a

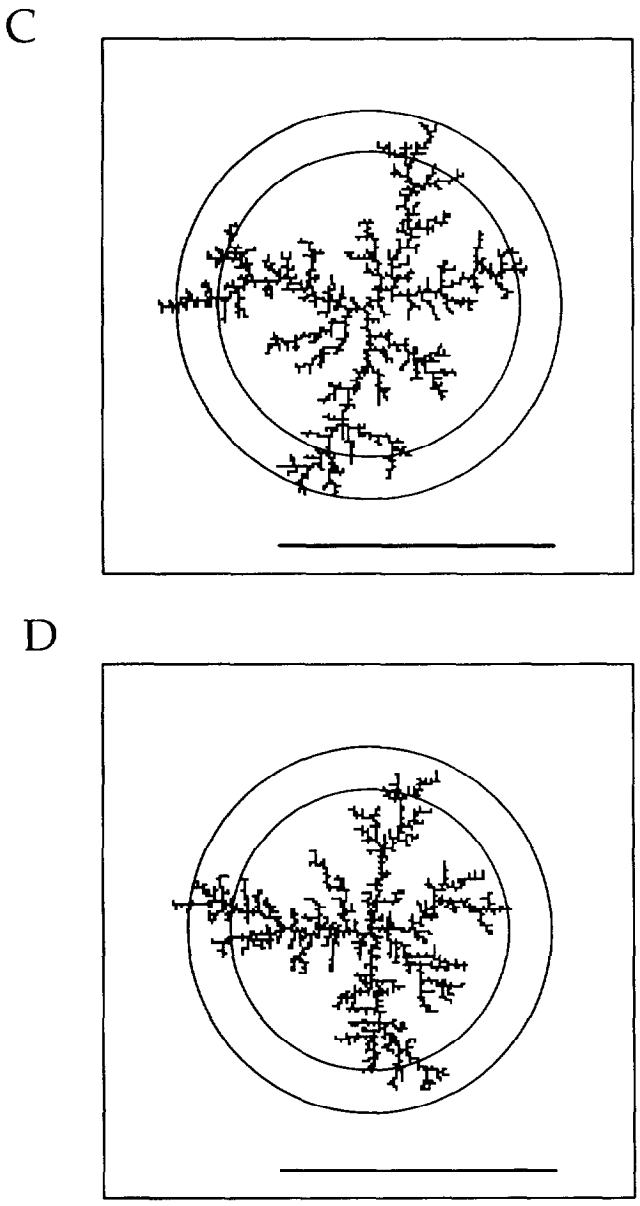

Figure 5. (C) and (D).

nearly constant amount (well after initiation), but more observations and a better theoretical understanding of the aggregation process will be required before the relationship between initial density and rate of aggregate growth can be definitively ascertained.

As to the radial growth and density of aggregates grown at different initial

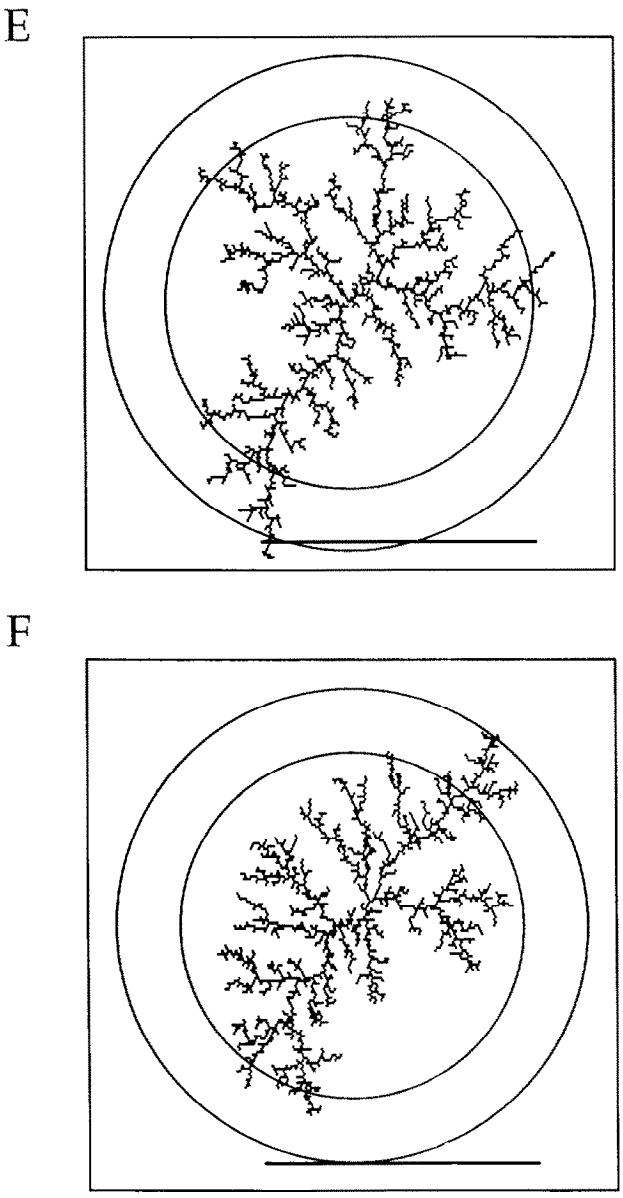

Figure 5. (E) and (F).

densities, matters appear fairly simple. Aggregates of similar mass were grown from three initial densities (25, 100 and 400 μm^{-2}; or 0.0016, 0.0064 and 0.0256 p^{-2}). The three simulation sets were run for different amounts of physiological time such that they all reached approximately the same mass (the number of elementary diffusion steps required for each simulation was

estimated from the mass vs time curves of Fig. 6). To facilitate interpretation of the data all simulations are construed as running for 60 "ticks", but of course the duration of a tick was different for the different densities (Fig. 7, legend). Figure 7A shows the mass as a function of time for the three densities. The masses are indistinguishable at 60 ticks precisely because the time dimension has been scaled to accomplish this. The similarity of the data over the entire time domain was not coerced, and so represents a legitimate observation. Figure 7B and C shows the radial growth rate and the radial density, respectively, for the three different initial densities. In both cases the different initial densities give the same results. Thus it appears that the only effect of particle density is to re-scale the time domain of the aggregation process.

5. Discussion. This report analyses both the growth rate and the structural properties of aggregates which are formed via density and diffusion limited aggregation (DDLA). Before discussing the findings it is worth reviewing the implicit and explicit assumptions inherent in this approach (and in the simpler DLA approach). First, the model assumes that the binding of membrane molecules is diffusion limited, so that a molecule binds with high probability upon diffusing laterally to a suitable location. Although not true of binding in solution (Northrup and Erickson, 1992), this is probably a better approximation in the case of membrane components because the rotational diffusion rate is typically large compared to the translational diffusion rate (Edidin, 1987). It is in any event the standard assumption of DLA and has been adopted here for purposes of comparison; a simple modification of the simulation scheme would permit the study of binding events that are not strictly limited by lateral diffusion. Secondly the model assumes that the binding is irreversible. Although this is not true in general, it is probably a reasonable approximation for many aggregating molecules, particularly if the focus of attention is on early development of the aggregate (i.e. a time scale of minutes or less). A third assumption is that the aggregate structure is rigid: the model makes no account for the possibility that an arm of the structure (e.g. Fig. 5A) can bend and join a

---

Legend for pages 664–666

Figure 5. Examples of density and diffusion limited aggregates. Each figure displays a typical aggregate (a single simulation), the mean maximal radius (outer circle), and the mean accretion radius (inner circle) for eight simulations. A, valence 4: step geometry 4: scale 1. B, same: scale 4. Note that scale 4 simulations are somewhat more compact than the scale 1 simulations. C, valence 4: step geometry 8: scale 1. D, same: scale 4. There is considerably less difference between the scale 1 and scale 4 results when the step geometry is 8. E, valence 6: step geometry 6: scale 1. F, same: scale 4. The difference between scale 1 and scale 4 aggregates is quite modest. The asymptotic valence 4 simulations (B, D) are significantly more compact than the valence 6 simulations (F). Scale bars, 100 particle diameters.

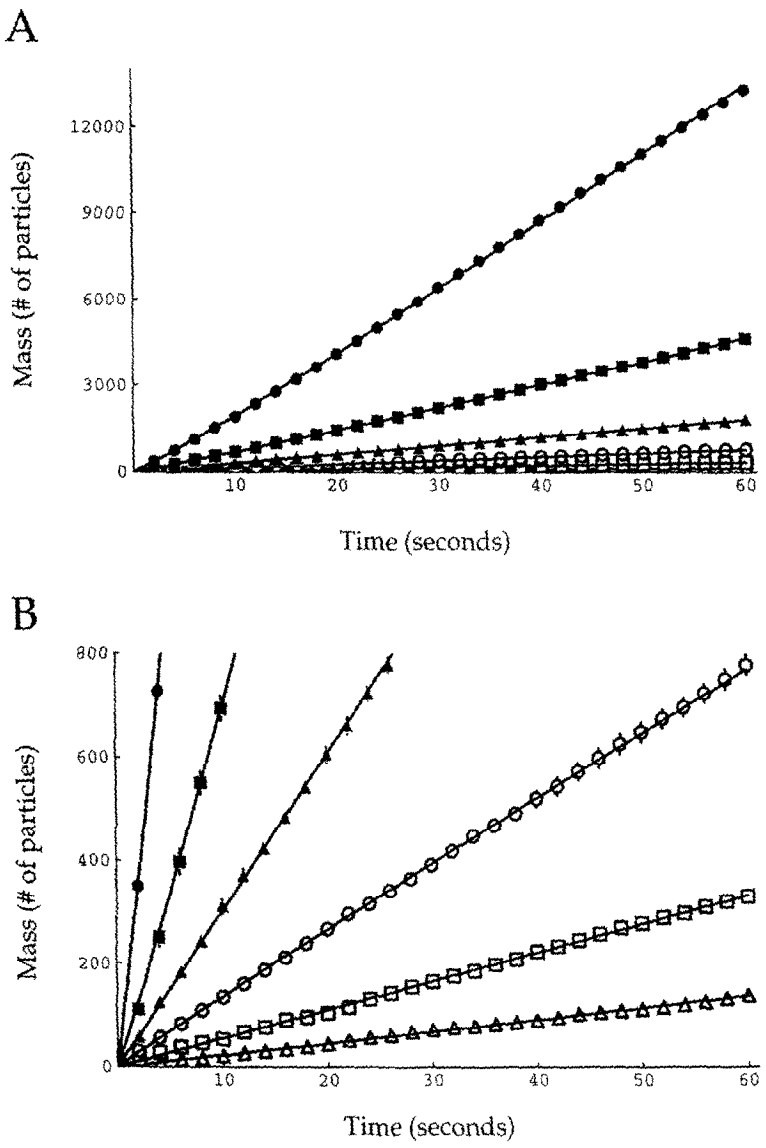

Figure 6. (A) and (B).

neighboring arm. This is probably a good approximation for small aggregates of relatively rigid components, but as they continue to enlarge this assumption almost certainly breaks down. Without specifying more about the nature of the bonds involved in a particular instance of aggregation we cannot predict how large an aggregate would have to be before the flexing of domains within the structure becomes an important factor. Fourthly there is the implicit assumption that no other processes which affect aggregate formation are taking place. Once again this assumption cannot be precisely true: it is well

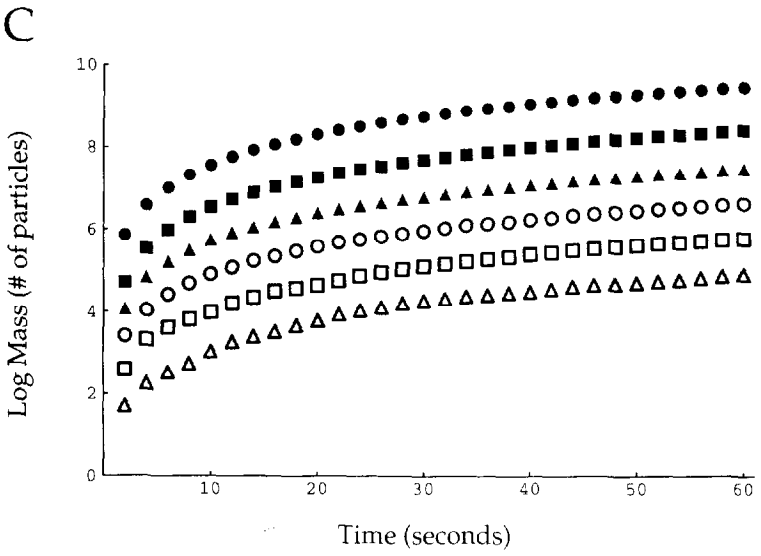

Figure 6. (C).

Figure 6. Comparison of the mass growth rate of density and diffusion limited aggregates grown at different particle densities. Mass (the number of particles in the aggregate) is plotted vs time (seconds of physiological time) for aggregates formed under different conditions. The simulations assume valence 4: step geometry 8: scale 4. Aggregates were formed with initial densities of 12.5 μm^{-2} (hollow triangles), 25 μm^{-2} (hollow squares), 50 μm^{-2} (hollow circles), 100 μm^{-2} (triangles), 200 μm^{-2} (squares), and 400 μm^{-2} (circles). Each point represents the mean and standard error of four simulations. All three figures represent the same data set. A–B, linear plots of the data over different ordinate ranges. C, log plot of the data in Fig. A and B. The curves in A and B represent Levenberg–Marquardt fits to $\text{mass}(t) = a \cdot t^b$. 12.5: $1.17 \cdot t^{0.54}$; 25: $2.00 \cdot t^{0.54}$; 50: $2.65 \cdot t^{0.59}$; 100: $4.10 \cdot t^{0.61}$; 200: $6.71 \cdot t^{0.62}$; 400: $12.0 \cdot t^{0.63}$.

known that membrane proteins undergo a cycle of insertion and turnover. Random insertion of molecules into the membrane will increase the density of bound molecules within the growing aggregate, while the removal of particles will tend to decrease the density and break the aggregate into smaller clusters. In the case of many molecules such as the acetylcholine receptor both of these processes are slow (membrane half-times on the order of hours), so that these effects can be safely ignored over the much shorter time scale examined here. Note that this will not be true in the case of molecules aggregating in coated pits. Finally there is an assumption in the present model that the aggregate structure is composed of one molecular species with homophilic binding; this of course need not be the case, but presents an interesting and relatively simple first case to consider.

In a more general sense the model also depends on the assumption that an unspecified event, which is local on the molecular scale, triggers aggregation.

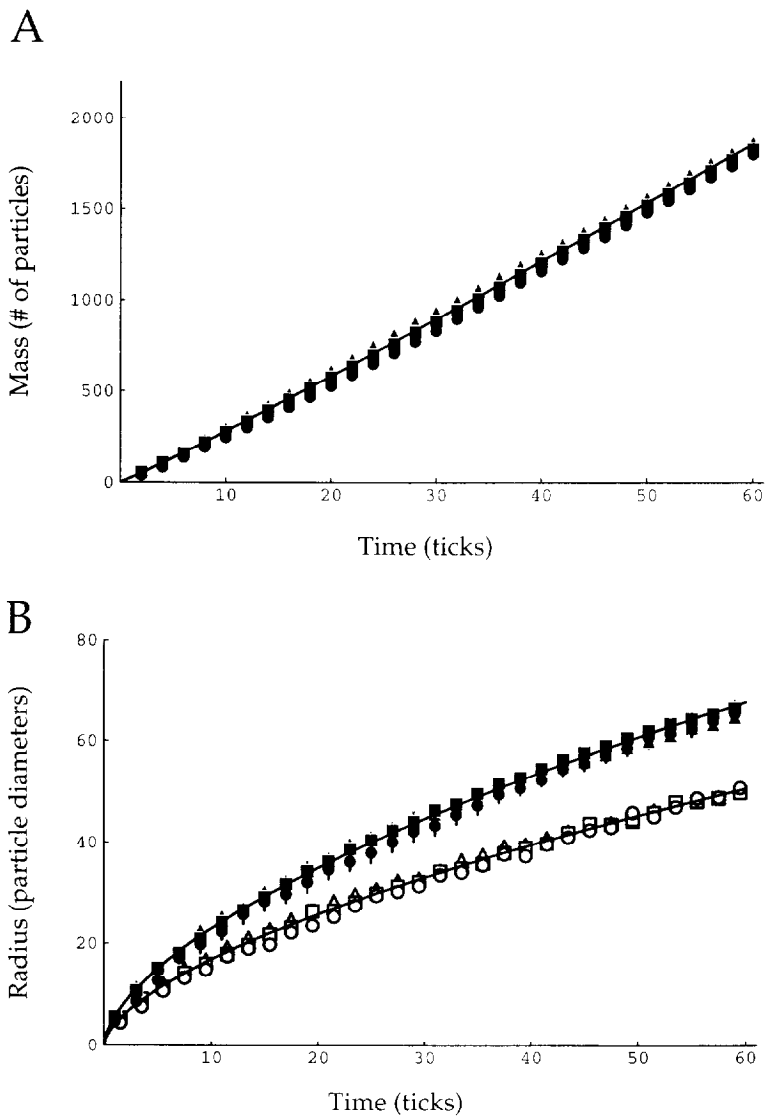

Figure 7. (A) and (B).

This assumption is plausible in the case of the acetylcholine receptor, where it has been suggested that the aggregation event may be triggered by locally activated tyrosine kinases (Wallace, 1991; Wallace *et al.*, 1991; Baker and Peng, 1993; Peng *et al.*, 1993; Wallace, 1994). On the other hand there may be processes in which aggregation is better thought of as triggered at random, multiple sites by the chance binding of adjacent molecules, as in cluster–cluster aggregation studies (Kolb *et al.*, 1983; Meakin, 1983; Saxton, 1992, 1993). It is worth noting that the former problem is a special case of the latter: if the initial

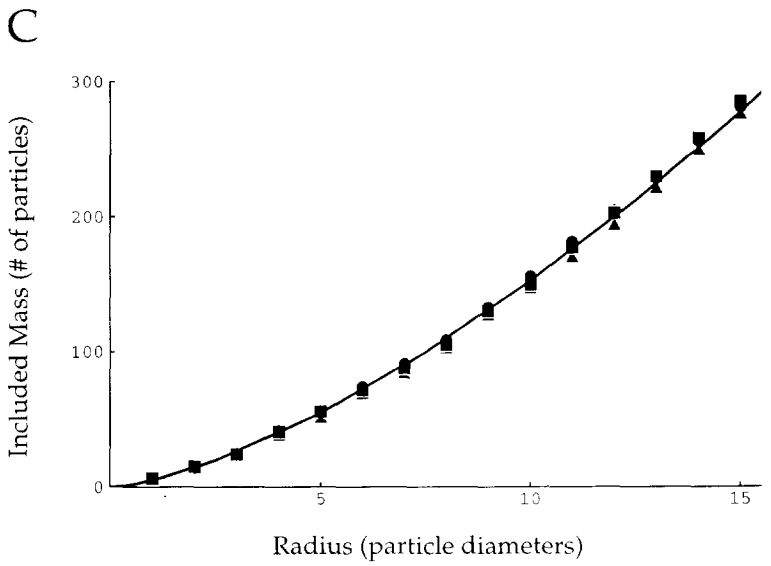

Figure 7. (C).

Figure 7. Comparison of the mass growth rate, radial growth rate and radial density of density and diffusion limited aggregates grown at different particles densities. The simulations assume valence 4: step geometry 8: scale 4. Aggregates were formed with initial densities of 25 μm^{-2} (triangles), 100 μm^{-2} (squares), and 400 μm^{-2} (circles). Each point represents the mean and standard error of eight simulations. Using the data of Fig. 6, these simulations were designed so that the different initial densities would reach approximately the same aggregate mass. This was accomplished by letting lower density simulations run for what corresponds to more physiological time. A, mass (the number of particles in the aggregate) vs time (in "ticks"; because the times scales for the three simulations are different the abscissa is represented in these arbitrary units for comparison purposes). The temporal scaling of these simulations has the effect of coercing the mass to be (approximately) the same as 60 ticks. Curve: $\text{mass}(t) = 24.5 \cdot t^{1.06}$, reduced $\chi^2 = 4.7$. B, radial growth (in particle diameters) vs time (in ticks). Both maximal radius (solid symbols) and mean accretion radius (hollow symbols) are shown. There are no significant differences in radial growth rate among the three different densities. Curves: radius $(t) = 5.75 \cdot t^{0.60}$, reduced $\chi^2 = 1.4$ (maximal radius): $\text{radius}(t) = 4.14 \cdot t^{0.61}$, reduced $\chi^2 = 2.6$ (mean accretion radius). C, included mass (number of particles within a circle of radius r, centered about the origin) vs r (radius in particle diameters). Curve: included $\text{mass}(r) = 5.11Z \cdot r^{1.48}$, reduced $\chi^2 = 3.4$.

density of sites in cluster–cluster models is low, the initial aggregates will be small and distant from each other, so that each individual cluster would be expected to grow according to the observations presented here.

Since the model assumptions are likely to be approximately true for a variety of membrane components, these assumptions represent the simplest and most plausible starting point from which to understand the diffusion limited aggregation of membrane molecules at a molecular level. This work is not

intended to advocate the general relevance of these assumptions, but rather to render these assumptions testable so that their relevance can be determined. The specific questions addressed concern the effects on the structure and growth of aggregates due to: (1) different diffusion modeling techniques; (2) changes in particle valence; and (3) changes in the initial density of particles.

5(a) *The effects of step geometry.* The effects of different approaches to modeling diffusion are illustrated by comparison of step geometry 4 vs step geometry 8 models for a valence 4 particle (Figs 2–5). The differences between these two approaches are small but significant; step geometry 8 simulations have a lower mass growth rate (Fig. 2A vs B), a lower spatial growth rate (Fig. 3A vs B), and a higher structure density (Fig. 4A vs B) than step geometry 4 simulations. All of these differences are diminished by scaling the diffusion process; scale 2 simulations show less difference due to step geometry, and at scale 4 these differences have nearly vanished (Figs 2–5). This scale-dependent convergence of results from the two step geometries is expected, as the Central Limit Theorem dictates that either approach to diffusion will converge to a bi-variate Gaussian as the scales increases. What is not clear *a priori* is how large a scale is required to achieve adequate approximation; the findings in this report indicate that a scale 4 simulation is sufficient to render the step geometry practically irrelevant as a simulation parameter.

What is the explanation for the observed differences that are seen, either between (scale 1) step geometry 4 and step geometry 8 results, or between scale 1 and scale 4 simulations of the same step geometry? At least part of the answer appears to be access to potential binding sites. Consider the aggregate structure depicted in Fig. 1A and B. The structure is identical—only the diffusion scale has been changed. Figure 1B (scale 2) shows a possible diffusion path for a free particle which results in its binding to an "inner" binding site. This same inner site is simply inaccessible in Fig. 1A (scale 1), because to reach it the particle has to first land on (and become bound to) an "outer" binding site. In a similar vein one can find structures in which (scale 1) inner sites are available if the step geometry is 8, but not if the step geometry is 4 (not shown). Thus it appears that the change from step geometry 4 to step geometry 8, or increased diffusion scaling, increases the accessibility of inner binding sites and results in a more dense structure.

Increasing the scale of valence 6 simulations has effects similar to those on valence 4 simulations, although the differences (scale 1 vs scale 4) are smaller (Figs 2–5). In fact the data support the conclusion that the change between scale 1 and scale 4 simulations is lowest for step geometry 6, intermediate for valence 4: step geometry 8, and largest for valence 4: step geometry 4. This is the same order in which the radial uniformity of the diffusion models would be ranked; step geometry 6 is more uniform than valence 4: step geometry 8,

which is more uniform than valence 4: step geometry 4. It is not surprising therefore that models consisting of a better (scale 1) approximation to a bivariate Gaussian show less change as the scale is increased.

5(b) *The effects of valence.* Having established conditions under which the step geometry can be ignored, we can now examine the effects of particle valence on model behavior. Valence 4 vs 6 simulations are compared in Figs 2–5. The most striking feature of these comparisons is that mass as a function of time is not much affected by valence (Fig. 2A,B vs C), while radial growth and structure density are quite dramatically changed (Figs 3–4A,B vs C). As an aggregate grows two opposing process effect future growth rate: (1) the binding of particles depletes the freely diffusing particles in the region about the aggregate; and (2) by virtue of growth, the sites available for binding are extended further from the origin toward the region of higher free particle density surrounding the aggregate (Stollberg, 1994). But the ratio of extension to particle depletion is higher in the less dense valence 6 aggregates than for the more dense valence 4 aggregates, since a lower density aggregate by definition depletes the particles less for each increment in radial growth. Thus one would expect a larger radial growth rate in the case of valence 6 particles. This qualitative explanation falls far short of explaining the observation that the larger radial growth of valence 6 particles nearly balances out their lower density, with the resulting effect that total mass as a function of time is approximately the same for the different valences. More analysis will be necessary to probe the exact nature and cause of this interaction.

5(c) *The effects of initial density.* One of the principal factors motivating this study of DDLA was the desire to predict how quickly membrane molecules would aggregate under the simple assumptions inherent in the model. The answer of course must depend on the diffusion constant and the initial density of molecule. As mentioned previously the diffusion constant only enters into the model as a proportionality constant relating the number of elementary diffusion steps to physiological time. Intuitively it is clear that the mass growth rate must increase with initial density, but there appears to be no simple quantitative accounting to be given for the effects of initial density. In particular one does not see a doubling of mass growth with a doubling of initial density (Fig. 6A,B). Figure 6C shows that the doubling of density appears to add an approximately fixed amount to log(mass) for time greater than 20 sec, but it should be stressed that this is simply an observation without theoretical support, and that it may not hold up over greater ranges in density.

As can be seen in the legend to Fig. 6, the mass growth rates for different densities do not differ solely in their scaling (or leading coefficient), but also in the exponent. This could be because the growth rates are truly different in form

for different initial densities, or simply because the aggregates compared in Fig. 6 are of quite different masses. To test these possibilities the data from Fig. 6 were used to estimate the time required to form aggregates of approximately equal mass at three different initial densities (25, 100 and 400 μm^{-2}; Fig. 7). It is shown that when the differences in mass growth rate are eliminated (Fig. 7A), the radial growth rate (Fig. 7B) and structure density (Fig. 7C) are the same within statistical error over this sixteen-fold range of particle density. This gives hope that some simple understanding of the effects of initial density may be available; the problem would appear more complicated if different initial densities led to radial growth rates and radial densities of different form even after scaling the temporal dimension.

5(d) *Overall comparison of DDLA to DLA.* The classical diffusion limited aggregation (DLA) model has been extensively studied, and it is in a real sense the parent of the density and diffusion limited aggregation (DDLA) model presented here. The DLA model does not incorporate time, density, or the diffusion constant, so that comparisons for much of the data presented here are not meaningful. The one exception is the radial density or fractal dimension of the resulting aggregates. Readers familiar with DLA will recall that the fractal dimension, which corresponds to the exponent in the curves of Fig 4, is found to be approximately 5/3. In a preliminary report it is stated that this value fits the DDLA data well (Stollberg, 1994), and yet the values given in the legend of Fig. 4 appear to be centered about approximately 1.5. It turns out that the value of this exponent in both DLAs and DDLAs depends somewhat on aggregate size. Because of the considerably larger computational load in simulating DDLA the aggregates presented here are quite small relative to many studies of DLA, and the simulations analysed in Fig. 4 are smaller than those used in the previous study (Stollberg, 1994). Accordingly, simulations of DLA were performed and analysed for fractal dimension within a radius of 15 particle diameters (like those of Fig. 4) and 60 particle diameters. The analyses limited to 15 diameters showed a fractal dimension of approximately 1.5, while the larger analyses gave values between 1.6 and 1.7 (data not shown), strengthening the interpretation that the apparent discrepancy is simply a matter of the size of the aggregate on which analysis is performed.

6. Summary and Conclusions. There are two important technical advances presented in this publication. First, the classical DLA model of aggregation has been extended to include particle density and diffusion constant, and so presents testable predictions about the rate of aggregation in a real system. Second, the modeling of the diffusion process has been significantly improved by the implementation of scale.

Using scaled diffusion it is shown that different schemes for implementing the elementary diffusion steps are, in effect, lesser or better approximations to a continuous diffusion probability. Moreover a diffusion scale of 4 renders either of the schemes addressed here a good approximation to continuous diffusion. Particle valence was shown to have a significant effect on aggregate structure and growth. Valence 6 simulations show larger radial growth rates, lower radial densities, and similar mass growth rates to those of valence 4. The effects of initial density on the outcome of density and diffusion limited aggregation appear to influence the time domain only; no differences in radial growth rate or radial density were observed when aggregates from different initial densities were grown to the same mass. Higher initial densities lead to more rapid aggregation, although the exact relationship between density and time remains to be understood.

Some of this approach has been presented in preliminary form (Stollberg, 1994). This work was supported by NIH grant #NS26943 and by a grant in computer time from the San Diego SuperComputing Center. I thank Dr J. B. Nation of the U.H. Mathematics Department for helpful discussions on this subject.

REFERENCES

Anderson, M. J. and M. W. Cohen. Nerve-induced and spontaneous redistribution of acetylcholine receptors on cultured muscle cells. *J. Physiol. (Lond).* **268**, 757–773.

Angelides, K. J., L. W. Elmer, D. Loftus and E. Elson. 1988. Distribution and lateral mobility of voltage-dependent sodium channels in neurons [published erratum appears in *J. Cell Biol.* (1989) May; **108**(5): preceding 2001]. *J. Cell Biol.* **106**, 1911–1925.

Axelrod, D., P. Ravdin, D. E. Koppel, J. Schlessinger, W. W. Webb, E. L. Elson and T. R. Podleski. 1976. Lateral motion of fluorescently labeled acetylcholine receptors in membranes of developing muscle fibers. *Proc. Natl. Acad. Sci. U.S.A.* **73**, 4594–4598.

Baker, L. P. and H. B. Peng. 1993. Tyrosine phosphorylation and acetylcholine receptor cluster formation in cultured Xenopus muscle cells. *J. Cell Biol.* **120**, 185–195.

Chao, N. M., S. H. Young and M. M. Poo. 1981. Localization of cell membrane components by surface diffusion into a "trap". *Biophys. J.* **36**, 139–153.

Dewey, T. G. and M. M. Datta. 1989. Determination of the fractal dimension of membrane protein aggregates using fluorescence energy transfer. *Biophys. J.* **56**, 415–420.

Dubinsky, J. M., D. J. Loftus, G. D. Fischbach and E. L. Elson. 1989. Formation of acetylcholine receptor clusters in chick myotubes: migration or new insertion? *J. Cell Biol.* 1733–1743.

Edidin, M. 1987. Rotational and lateral diffusion of membrane proteins and lipids: phenomena and function. In *Current Topics in Membranes and Transport*, pp. 91–119. Orlando: Academic Press.

Edwards, C. and H. L. Frisch. 1976. A model for the localization of acetylcholine receptors at the muscle endplate. *J. Neurobiol.* **7**, 377–381.

Gershon, N. D. 1978. Model for capping of membrane receptors based on boundary surface effects. *Proc. Natl. Acad. Sci. U.S.A.* **75**, 1357–1360.

Joe, E. and K. J. Angelides. 1993. Clustering and mobility of voltage-dependent sodium channels during myelination. *J. Neurosci.* **13**, 2993–3005.

Kolb, M., R. Botet and R. Jullien. 1983. Scaling of kinetically growing clusters. *Phys. Rev. Lett.* **51**, 1123–1126.

Kusumi, A., Y. Sako and M. Yamamoto. 1993. Confined lateral diffusion of membrane receptors as studied by single particle tracking (nanovid microscopy). Effects of calcium-induced differentiation in cultured epithelial cells. *Biophys. J.* **65**, 2021–2040.

Mandelbrot, B. B. and C. J. G. Evertsz. 1990. The potential distribution around growing fractal clusters. *Nature* **348**, 143–145.

Meakin, P. 1983. Formation of fractal clusters and networks by irreversible diffusion-limited aggregation. *Phys. Rev. Lett.* **51**, 1119–1122.

Meakin, P. 1987. Noise-reduced diffusion-limited aggregation. *Phys. Rev. A* **36**, 332–339.

Moreira, F., R. R. Freire and C. M. Chaves. 1989. Scaling laws for the noise-reduced diffusion-limited aggregation. *Phys. Rev. A* **40**, 2225–2228.

Muthukumar, M. 1983. Mean-field theory for diffusion-limited cluster formation. *Phys. Rev. Let.* **50**, 839.

Northrup, S. H. and H. P. Erickson. 1992. Kinetics of protein–protein association explained by Brownian dynamics computer simulation. *Proc. Natl. Acad. Sci. U.S.A.* **89**, 3338–3342.

Ossadnik, P. 1991. Multiscaling analysis of large-scale off-lattice DLA. *Physica A* **176**, 454–462.

Peng, H. B., L. P. Baker and Z. Dai. 1993. A role of tyrosine phosphorylation in the formation of acetylcholine receptor clusters induced by electric fields in cultured Xenopus muscle cells. *J. Cell Biol.* **120**, 197–204.

Poo, M.-m. 1982. Rapid lateral diffusion of functional ACh receptors in embryonic muscle cell membrane. *Nature* **295**, 332–335.

Sander, L. M. 1986. Fractal growth processes. *Nature* **322**, 789–793.

Saxton, M. J. 1992. Lateral diffusion and aggregation. A Monte Carlo study. *Biophys. J.* **61**, 119–128.

Saxton, M. J. 1993. Lateral diffusion in an archipelago. Dependence on tracer size. *Biophys. J.* **64**, 1053–1062.

Stenberg, M. and H. Nygren. 1991. Computer simulation of surface-induced aggregation of ferritin. *Biophys. Chem.* **41**, 131–141.

Stollberg, J. 1994. A model for diffusion-limited aggregation in membranes. *Com. Mol. Cell. Biophys.* **8**, 188–198.

Stollberg, J. and S. E. Fraser. 1988. Acetylcholine receptors and concanavalin A-binding sites on cultured Xenopus muscle cells: electrophoresis, diffusion, and aggregation. *J. Cell. Biol.* **197**, 1397–1408.

Stollberg, J. and S. E. Fraser. 1990. Local accumulation of acetylcholine receptors is neither necessary nor sufficient to induce cluster formation. *J. Neurosci.* **10**, 247–255.

Stollberg, J. and H. Gordon. 1992. Diffusion-trapping of acetylcholine receptors: a numerical model. *Invited Seminar* (Keystone Symposia: Synapse formation and function: The neuromuscular junction and the central nervous system).

Tokuyama, M. and K. Kawasaki. 1984. Fractal dimensions for diffusion-limited aggregation. *Phys. Lett.* **100A**, 337–340.

Wallace, B. G. 1991. The mechanism of agrin-induced acetylcholine receptor aggregation. *Philos. Trans. R. Soc. Lond. [Biol.]* **331**, 273–280.

Wallace, B. G. 1994. Staurosporine inhibits agrin-induced acetylcholine receptor phosphorylation and aggregation. *J. Cell. Biol.* **125**, 661–668.

Wallace, B. G., Z. Qu and R. L. Huganir. 1991. Agrin induces phosphorylation of the nicotinic acetylcholine receptor. *Neuron* **6**, 869–878.

Weaver, D. L. 1983. Diffusion-mediated localization on membrane surfaces. *Biophys. J.* **41**, 81–86.

Witten, T. A., Jr. and P. Meakin. 1983. Diffusion-limited aggregation at multiple growth sites. *Phys. Rev. B.* **28**, 5632–5642.
Witten, T. A. and L. M. Sander. 1981. Diffusion-limited aggregation, a kinetic critical phenomenon. *Phys. Rev. Lett.* **47**, 1400–1403.

Received 20 November 1994
Revised version accepted 28 February 1995